ACS APPLIED ENERGY MATERIALS

www.acsaem.org Article

Addressing the Origin of Photocurrents and Fuel Production Activities in Catalyst-Modified Semiconductor Electrodes

Brian L. Wadsworth, Nghi P. Nguyen, Daiki Nishiori, Anna M. Beiler, and Gary F. Moore*

Cite This: *ACS Appl. Energy Mater.* 2020, 3, 7512–7519 Read Online

ACCESS | Metrics & More | Article Recommendations | Supporting Information

ABSTRACT: The direct integration of electrocatalysts with photovoltaic materials provides a strategy to photoelectrochemically power chemical transformations and store intermittent solar energy as fuels. However, many electrocatalytic components used or proposed for use in such assemblies also absorb visible light. This prompts the questions: to what extent does a selected electrocatalytic coating screen photons from reaching the underlying photovoltaic, do excited-state species associated with coating layers contribute to photocurrent production via mechanisms involving dye-sensitization processes, and are relatively high or low loadings of catalytic sites advantageous. Herein, we highlight how optical and electrochemical characterization techniques can be coupled with structural information to address these questions. The experiments described in this work make use of a p-type gallium phosphide semiconductor that is interfaced with cobalt porphyrin hydrogen evolution reaction catalysts. However, the experimental techniques and discussions presented in this work can likely be applied to other materials and chemical transformations, providing a general yet useful strategy for better understanding the origin of photocurrents and fuel production activities in catalyst-modified semiconductor electrodes.

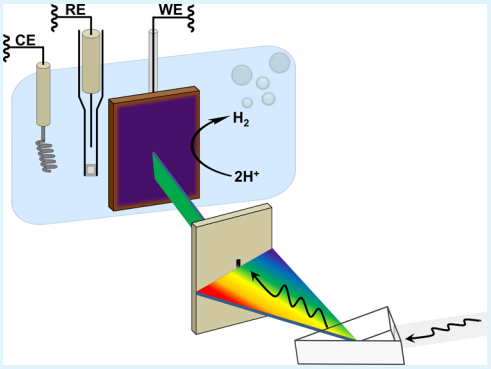

KEYWORDS: *photoelectrosynthesis, molecular-modified semiconductors, quantum efficiency, light harvesting efficiency, porphyrins*

1. INTRODUCTION

Photoelectrosynthesis provides an approach to capture, convert, and store solar energy in the form of chemical bonds.[1−3] However, the ability to effectively interface electrocatalysts for activating multielectron/multiproton chemical transformations with materials that absorb sun light and convert photons into charge carriers moving through a potential remains challenging.[4−8] Additionally, most electrocatalyst layers also absorb visible light, complicating analysis of these composite materials and determination of the components directly involved in energy harvesting.

We have previously reported synthetic methods for interfacing molecular cobalt porphyrin catalysts with (semi)conducting materials.[9−12] In one example, cobalt porphyrins are immobilized onto gallium phosphide (GaP) semiconductors using a two-step strategy involving initial UV-induced grafting of 4-vinylpyridine, to form polypyridyl coatings (PPy) on GaP surfaces, followed by wet-chemical processing with a solution of 5,10,15,20-tetra-*p*-tolylporphyrin cobalt(II) (CoTTP). This overall process yields samples where the porphyrin cobalt centers are coordinated to pyridyl nitrogen sites of the polymeric coating (Scheme 1).

Porphyrins are effective electrocatalysts, capable of transforming protons to hydrogen or reducing carbon dioxide to carbon monoxide and other reduced forms of carbon.[13−18] For this latter reason, they have been utilized as components in

Scheme 1. Schematic Diagram Highlighting the Molecular Structure of a Cobalt Porphyrin Coordinated to a Surface-Grafted Polypyridyl Chain on a CoTTP|PPy|GaP Working Electrode Wired in a Three-Electrode Configuration under Illumination Using a Broadband or Monochromatic Light Source

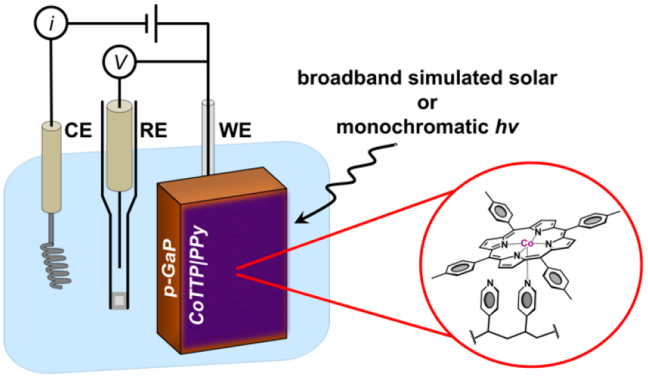

Received: April 21, 2020
Accepted: June 29, 2020
Published: June 29, 2020

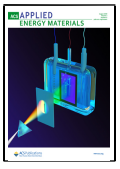

https://dx.doi.org/10.1021/acsaem.0c00919
ACS Appl. Energy Mater. 2020, 3, 7512–7519

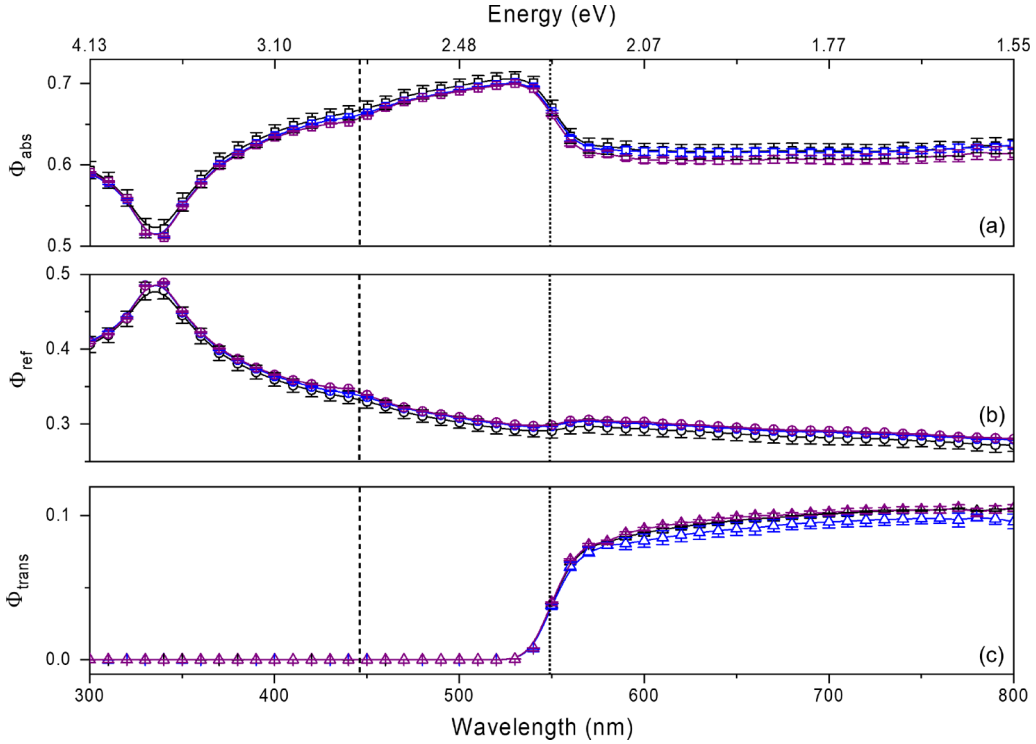

Figure 1. Plots of the (a) probability of absorption (Φ_{abs}; squares), (b) probability of reflection (Φ_{ref}; circles), and (c) probability of transmission (Φ_{trans}; triangles) measured using GaP (black), PPy|GaP (blue), and CoTTP|PPy|GaP (purple) versus the wavelength of illumination. The dashed and dotted black lines indicate energies associated with the direct and indirect band gaps of GaP, respectively.

electrocatalytic and photoelectrosynthetic assemblies.[8−12,19−21] The relatively high extinction coefficients of tetrapyrrolic macrocycles, including porphyrins (10^3 to 10^5 M^{-1} cm^{-1} across the visible region of the electromagnetic spectrum), have also made them useful as light-harvesting components in biological and technological systems, including applications in dye-sensitized solar cells.[22−29]

GaP has also been explored as a light-absorbing material for applications in photoelectrochemistry.[30−38] Favorable aspects of GaP semiconductors include conduction band energetics (∼−1 V vs NHE at pH 1)[39] with sufficient redox poise for driving reductive chemical transformations, including proton and CO_2 reduction, but surface corrosion and ineffective transfer of minority carriers across the semiconductor|liquid interface limit its performance.[40] Although chemical modification of semiconductor surfaces can improve rates of photoelectrosynthetic fuel production (Supporting Information Scheme S1a), the addition of colored materials, which include myriad electrocatalysts, can also confer the undesirable effect of reflecting or parasitically absorbing photons before they can reach the underlying semiconductor (Scheme S1b).[9−11,19−21,41−43]

Juxtaposed with more traditional approaches of maximizing the per geometric area loading of catalysts to achieve higher activities, design strategies can be more nuanced in the case of photoelectrosynthetic assemblies and relatively thick catalyst layers can hamper performance by screening light and/or disfavoring accumulation of redox equivalents at individual catalytic sites. For example, studies involving photoactivation of a semiconductor co-modified with a molecular dye and a proxy for a molecular catalyst indicate relatively low loadings of catalytic sites could be propitious in photoelectrosynthetic applications.[44,45] Conversely, dye-sensitization processes involving the transfer of charge carriers between excited dyes and semiconductors (Scheme S1c) have been reported as a strategy for extending the absorption range of semiconducting materials, including GaP, and thereby improving their photoelectrochemical performance.[46−51]

Previous work from our group shows that when wired in a three-electrode configuration with appropriate counter and reference electrodes (Scheme 1), cobalt porphyrin−polypyridyl-modified GaP electrodes (CoTTP|PPy|GaP) use light to power the production of hydrogen gas from pH neutral aqueous solutions in the absence of sacrificial chemical reductants, and with no electrochemical forward biasing, at a rate of ∼10 μL of H_2 min^{-1} cm^{-2}.[9] Complementary methods of ellipsometry, inductively coupled plasma mass spectrometry, and X-ray photoelectron spectroscopy were used to quantify the thickness of the polypyridyl films, the per geometric area loading of cobalt porphyrins, and the fraction of pyridyl sites coordinated to cobalt porphyrin centers.[9] Given this structural information and the near-unity faradaic efficiency determined by product analysis, the hydrogen production rate of 10 μL of H_2 min^{-1} cm^{-2} equates to a per-cobalt-site hydrogen evolution reaction (HER) activity of 17.6 H_2 molecules s^{-1} Co^{-1}.[9] More recently, we developed kinetic models relating the HER activity of these photoelectrodes to the fraction of catalysts present in their activated form under varying intensities of steady-state illumination.[11] Herein, we now show that quantification of the per geometric area loading of molecular components can be coupled with information on their light harvesting efficiency (LHE)[52] and overall external quantum efficiency (EQE)[53−55] to quantify the fraction of photons absorbed by surface-grafted molecular coatings and address the effects this can have on overall photocurrent production and associated rates of photoelectrosynthetic fuel production.

https://dx.doi.org/10.1021/acsaem.0c00919
ACS Appl. Energy Mater. 2020, 3, 7512−7519

2. EXPERIMENTAL SECTION

2.1. Sample Preparation. Functionalization of GaP surfaces with polypyridyl coatings containing cobalt porphyrin units has been previously reported (see the Supporting Information for further details).[9]

2.2. UV−Vis−Near-IR. All ultraviolet−visible−near-infrared (UV−vis−NIR) optical spectra were recorded using a SolidSpec-3700 UV−vis−NIR spectrophotometer (Shimadzu, Kyoto, Japan) with a D_2 (deuterium) lamp for the ultraviolet range and a WI (halogen) lamp for the visible and near-infrared ranges. All solution-based measurements were performed using a quartz cuvette sealed under air and chloroform as a solvent. The data were collected at 0.5 nm intervals (see the Supporting Information for further details). All solid-state optical measurements, including those involving samples prior to and following chemical-modification steps, were performed using 400 μm thick GaP wafers (see the Supporting Information for further details). All measurements were performed using three samples of GaP (cut from the same wafer) that were characterized at each step of the surface-modification procedure, and the reported values are the averaged values.

2.3. Photoelectrochemistry. All photoelectrochemical measurements were performed using a three-electrode configuration as previously described (see the Supporting Information for further details).[11] At least three electrodes were characterized for each construct, and the reported values are the averaged values.

2.4. External Quantum Efficiency Measurements. External quantum efficiencies were measured following a previously reported procedure (see the Supporting Information for further details).[11] At least three electrodes were characterized for each construct, and the reported values are the averaged values.

2.5. Internal Quantum Efficiency Measurements. Internal quantum efficiencies (IQEs)[56] were calculated by dividing the EQE at each wavelength by the LHE at each wavelength.[57] The LHE at each wavelength was determined using a previously reported method (see the Supporting Information for further details).[11] At least three electrodes were characterized for each construct, and the reported values are the averaged values.

3. RESULTS AND DISCUSSION

3.1. Optical Characterization. Measurements of the wavelength-resolved probability of absorption (Φ_{abs}),[52] probability of reflection (Φ_{ref}), and probability of transmission (Φ_{trans}) collected using samples of GaP, polypyridyl-modified GaP (PPy|GaP), or CoTTP|PPy|GaP, are indicated in Figure 1. For all three constructs, the transmittance at wavelengths with corresponding energies greater than the indirect band gap of GaP (≤549 nm, ≥2.26 eV) is ∼0. Further, the reflection and absorption spectra recorded in this spectral region are nearly identical (that is, with values that overlap within the error of the measurements), except for relatively small differences in Φ_{ref} and Φ_{abs} recorded at 440 nm (where the respective values are as follows: 0.336 ± 0.007 and 0.664 ± 0.007 for samples of GaP, 0.342 ± 0.001 and 0.658 ± 0.001 for samples of PPy|GaP, and 0.347 ± 0.001 and 0.653 ± 0.001 for samples of CoTTP|PPy|GaP; Figure S1). These results indicate the differences in both Φ_{ref} and Φ_{abs} at 440 nm is <1% between samples of CoTTP|PPy|GaP, PPy|GaP, and GaP.

Optical measurements performed at wavelengths from 549 nm up to 800 nm show the Φ_{trans} values recorded using all three constructs approach 11% at relatively longer wavelengths (Figure 1). Further, the Φ_{abs} values recorded in this spectral region are nonzero, even though photons at these wavelengths have corresponding energies less than the indirect band gap of GaP. Absorption at these longer wavelengths is attributed to free-carrier (holes in the case of this p-type semiconductor) absorption in GaP.[58] Related to this, the absorption coefficients of CoTTP|PPy|GaP samples at wavelengths >549 nm are significantly lower than those measured using samples of GaP or PPy|GaP (Figure 2), indicating there is a reduction

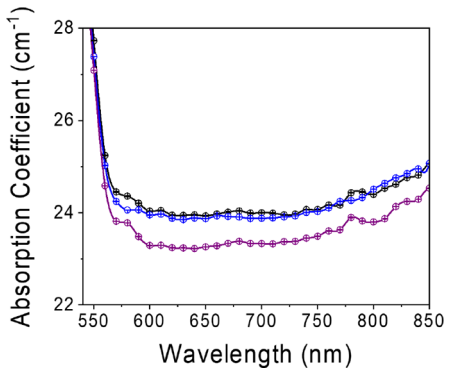

Figure 2. Plots of the absorption coefficients measured using GaP (black), PPy|GaP (blue), and CoTTP|PPy|GaP (purple) versus the wavelength of illumination. Error bars are included for each data point shown.

in the free-carrier population following immobilization of the porphyrins. Because porphyrins are redox active and p-type doping of a semiconductor introduces free-carrier holes that are associated with an increase in the potential of the semiconductor Fermi level, we postulate this decrease in sub-band gap absorption coefficients results in part from an equilibration of the potentials associated with the isolated p-type semiconductor and cobalt porphyrin layer. During this equilibration, carriers flow between the semiconductor and porphyrin layer until equilibrium is established and there is no potential difference across the interface.

3.2. Photoelectrochemical Characterization. Linear sweep voltammograms recorded under broadband simulated solar illumination using working electrodes immersed in pH neutral aqueous conditions (0.1 M phosphate buffer) are shown in Figure 3. Under these experimental conditions, electrodes constructed from samples of GaP, PPy|GaP, and CoTTP|PPy|GaP yield current densities of 0.50 ± 0.07, 0.68 ± 0.06, and 0.84 ± 0.04 mA cm^{-2}, respectively, when operating at the equilibrium potential of the H^+/H_2 couple (0 V vs the

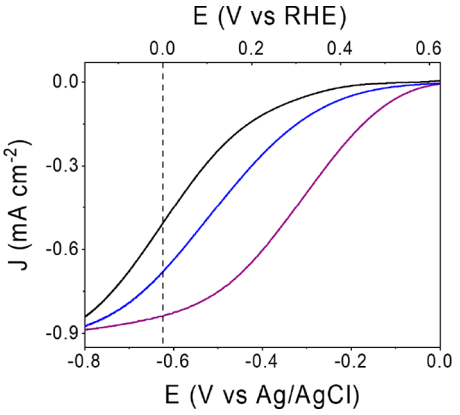

Figure 3. Linear sweep voltammograms recorded using a GaP (black solid), PPy|GaP (blue solid), or CoTTP|PPy|GaP (purple solid) electrode in 0.1 M phosphate buffer (pH 7) under simulated 1-sun illumination. The vertical dashed line at 0 V vs RHE indicates the equilibrium potential of the H^+/H_2 couple.

https://dx.doi.org/10.1021/acsaem.0c00919
ACS Appl. Energy Mater. 2020, 3, 7512−7519

reversible hydrogen electrode [RHE]). Additional metrics, including open-circuit potentials and associated fill factors, are included in Table S1.

In addition to measurements performed under broadband illumination, wavelength-resolved external quantum efficiencies were recorded using either PPy|GaP or CoTTP|PPy|GaP working electrodes (Figure 4a) polarized at 0 V vs RHE in pH

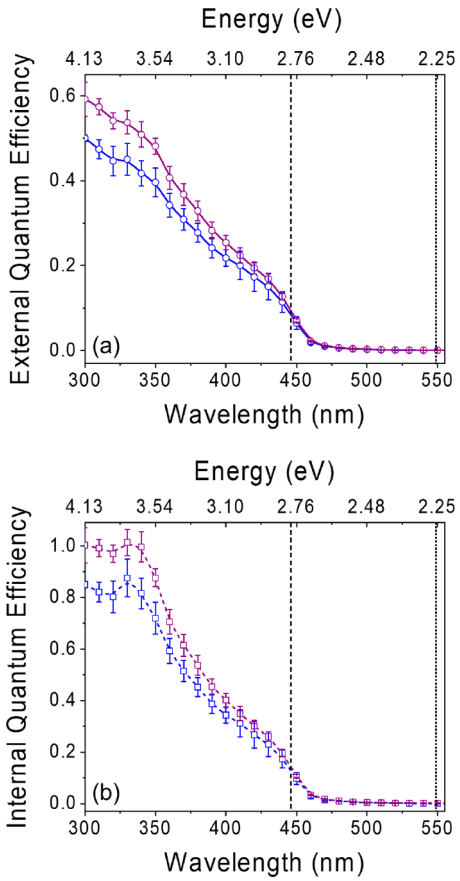

Figure 4. (a) External and (b) internal quantum efficiency action spectra recorded using PPy|GaP (blue) or CoTTP|PPy|GaP (purple) electrodes polarized at 0 V vs RHE in 0.1 M phosphate buffer (pH 7). The dashed and dotted black lines indicate energies associated with the direct and indirect band gaps of GaP, respectively.

neutral aqueous conditions (EQE action spectra of unmodified GaP samples are not included due to the instability of these samples on the time scales required to conduct EQE measurements). Under these experimental conditions, the photocurrents recorded when illuminating either PPy|GaP or CoTTP|PPy|GaP electrodes at wavelengths ≲549 nm are nonzero (consistent with the 2.26 eV indirect band gap of GaP) and rise sharply when illuminating at wavelengths <446 nm, where the transition from the indirect to the direct band gap occurs (2.78 eV). Further, the EQE action spectra of both PPy|GaP and CoTTP|PPy|GaP reach maxima at 300 nm, albeit with values of 50% and 59%, respectively. The EQEs and LHEs measured using PPy|GaP and CoTTP|PPy|GaP electrodes enable construction of IQE plots (Figure 4b) that both display maxima at 330 nm, with values of 88% for PPy|GaP and 100% for CoTTP|PPy|GaP.

To confirm that current densities recorded under monochromatic lighting conditions and constant potential polarization (0 V vs RHE) are consistent with those measured under broadband illumination when sweeping the applied potential, wavelength-resolved electron flux plots (Figure 5)

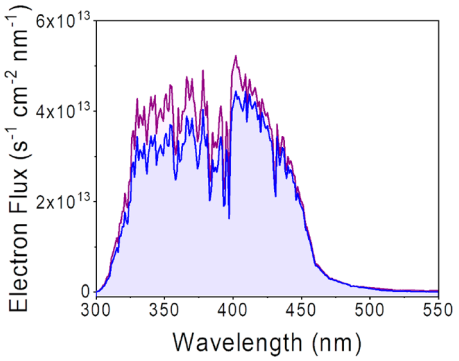

Figure 5. Electron flux spectra associated with PPy|GaP (blue) or CoTTP|PPy|GaP (purple) electrodes polarized at 0 V vs RHE in 0.1 M phosphate buffer (pH 7). All plots were generated using the related external quantum efficiency data and considering illumination under air mass 1.5 global tilt solar flux. At the equilibrium potential (0 V vs RHE) the activities associated with both the PPy|GaP and CoTTP|PPy|GaP electrodes are approaching their limiting values (see Figure 3).

were generated using the EQE data shown in Figure 4a and either the photon flux associated with the air mass 1.5 global tilt (AM 1.5 G) spectrum (Figure S10)[59] or the photon flux associated with the spectral profile of the solar simulator used in our experiments (Figure S10). Integration of the electron flux plots associated with AM 1.5 G illumination conditions yield values of 0.71 ± 0.06 mA cm^{-2} for the PPy|GaP electrodes and 0.83 ± 0.05 mA cm^{-2} for the CoTTP|PPy|GaP electrodes. Integration of the electron flux plots associated with the simulated solar conditions yield values of 0.77 ± 0.06 mA cm^{-2} for the PPy|GaP electrodes and 0.90 ± 0.05 mA cm^{-2} for the CoTTP|PPy|GaP electrodes. Thus, the current densities obtained from integration of the electron flux plots are consistent when using either AM 1.5 G conditions or the lamp spectrum of the solar simulator used in our experiments (Table S2). Further, within the experimental error of these measurements, the current densities determined by integration of the wavelength-resolved electron flux plots are consistent with those measured in linear sweep voltammograms recorded using broadband simulated solar illumination.

3.3. Comparisons between Heterogeneous−Homogeneous Semiconductor Electrodes and Homogeneous Solutions Containing the Molecular Electrocatalyst. The LHE and EQE action spectra of PPy|GaP prior to and following porphyrin modification were also compared with absorption spectra recorded using solutions of CoTTP in chloroform in the absence and presence of pyridine (Figures 6, S3, and S5). These comparisons yield insights regarding to what extent and at what wavelengths the presence of cobalt porphyrin units immobilized on GaP surfaces could attenuate the photon flux reaching the underlying GaP semiconductor and possibly contribute to photocurrent densities at wavelengths with corresponding energies that are lower than the 2.26 eV band gap of GaP.

Absorption spectra of CoTTP in chloroform are characterized by a relatively strong Soret absorption at 412 nm ((2.2 ± 0.1) × 10^5 M^{-1} cm^{-1}) and a weaker Q-type absorption at 530 nm ((1.6 ± 0.1) × 10^4 M^{-1} cm^{-1}) with both absorption features appearing at wavelengths where the underlying GaP is

https://dx.doi.org/10.1021/acsaem.0c00919
ACS Appl. Energy Mater. 2020, 3, 7512−7519

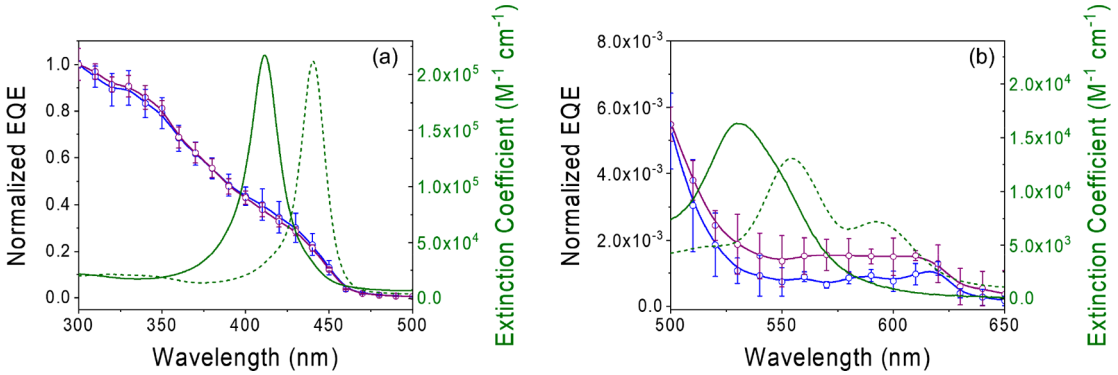

Figure 6. External quantum efficiency action spectra recorded using PPy|GaP (blue) or CoTTP|PPy|GaP (purple) electrodes polarized at 0 V vs RHE in 0.1 M phosphate buffer (pH 7) normalized at 300 nm as well as absorption spectra of 5,10,15,20-tetra-*p*-tolylporphyrin cobalt(II) (CoTTP) recorded in chloroform in the absence (solid green) and presence of ∼1 equiv of pyridine (dashed green) in the wavelength ranges where the porphyrin (a) Soret absorption (300−500 nm) and (b) Q-type absorptions (500−650 nm) occur.

photoactive (Figure S3 and Table S4). In contrast, spectra of CoTTP recorded in chloroform following the addition of ∼1 equiv of pyridine show two Q-type absorption maxima at 554 nm ($(1.3 \pm 0.1) \times 10^4$ M^{-1} cm^{-1}) and 592 nm ($(7.2 \pm 0.5) \times 10^3$ M^{-1} cm^{-1}) (i.e., wavelengths with corresponding energies that are lower than the 2.26 eV band gap of GaP) and a Soret absorption maximum centered at 441 nm ($(2.1 \pm 0.2) \times 10^5$ M^{-1} cm^{-1}) (Scheme S2, Figure S3, and Table S4).[60] The Soret absorption in the presence of pyridine occurs at a wavelength where there is a relatively small difference (0.5 ± 0.1%) in LHEs recorded at 440 nm using samples of PPy|GaP or CoTTP|PPy|GaP (Figure S5).[61] In addition to the optical data presented in this article, obtained using either heterogeneous−homogeneous samples of cobalt porphyrin-modified GaP semiconductors or homogeneous solutions of cobalt porphyrins, we have previously reported on the optical and electrochemical properties of heterogeneous−homogeneous samples of cobalt porphyrins immobilized on nanostructured transparent conducting oxide materials.[12] These previous studies indicate the optical properties of the CoTTP|PPy layer (including wavelengths of the Soret and Q-type absorption features and their corresponding extinction coefficients) track closely with those recorded using homogeneous solutions containing cobalt porphyrin and pyridine (Figure S4 and Table S5).

The fraction of light absorbed by surface-grafted cobalt porphyrins in samples of CoTTP|PPy|GaP was approximated using the extinction coefficients recorded for homogeneous solutions of CoTTP in chloroform following the addition of ∼1 equiv of pyridine ($(2.1 \pm 0.2) \times 10^5$ M^{-1} cm^{-1} for the Soret absorption maximum and $(1.3 \pm 0.1) \times 10^4$ M^{-1} cm^{-1} and $(7.2 \pm 0.5) \times 10^3$ M^{-1} cm^{-1} for the Q-type absorption maxima), the per geometric area loading of cobalt porphyrin in samples of CoTTP|PPy|GaP (∼1 nmol cm^{-2}), and the polypyridyl film thickness (4 ± 1 nm). Analyses of these approximated LHEs indicate the immobilized porphyrins attenuate ∼39% of the light at the Soret absorption maximum (441 nm), ∼3% of the light at the most intense Q-type absorption maximum (554 nm), and ∼2% of the light at the lower intensity Q-type absorption maximum (592 nm) (Figure S6; see the Supporting Information for further details). However, despite any attenuation of light by the porphyrins, the overall photocurrents and related EQEs measured using CoTTP|PPy|GaP working electrodes are higher than those measured using PPy|GaP electrodes.

Comparisons of the spectral profiles associated with the EQE action spectra recorded using PPy|GaP or CoTTP|PPy|GaP electrodes address to what extent the porphyrin coating may enhance photoelectrosynthetic performance by mechanisms involving dye sensitization. Following normalization at 300 nm, a wavelength that is well resolved from the cobalt porphyrin Soret and Q-type absorptions, and where EQEs of PPy|GaP and CoTTP|PPy|GaP are at maximum values, these plots show no significant differences (i.e., outside the error of the measurements) in spectral intensities at wavelengths associated with cobalt porphyrin Soret absorption (Figure 6a) as well as the Q-type absorptions (Figure 6b). Although cobalt porphyrin complexes featuring coordination to axial pyridyl moieties display Q-type absorptions at wavelengths with energies lower than the band gap of GaP (>549 nm, <2.26 eV),[12,62−64] there is an absence of prominent sub-band gap features in EQE action spectra recorded using CoTTP|PPy|GaP samples. Analysis of EQEs recorded in the 570−610 nm range does indicate a slight (i.e., outside the error of the measurements) increase of the normalized signal intensity associated with the porphyrin-modified GaP electrodes (Figure 6b), but this difference in signal accounts for only 0.05% of the total current density measured under broadband illumination conditions. Although the electronic spectra of porphyrins recorded in the absence of polarization may not be indicative of the steady-state concentration of porphyrin species present on GaP surfaces under the conditions in which EQEs are measured (i.e., steady-state illumination and polarization at 0 V vs RHE in the presence of chemical substrates), these results confirm the immobilized porphyrins serve relatively little role in extending the photoactivity of the hybrid assemblies to wavelengths outside the actinic range of GaP.

3.4. Apparent Dye-Contribution Efficiencies. The LHEs associated with the cobalt porphyrin−polypyridyl surface coating were also used to generate hypothetical EQE plots. These plots are constructed assuming the immobilized porphyrins serve strictly as light-screening pigments or dye sensitizers (not catalysts). The hypothetical EQE plots thus represent extreme conditions where all cobalt porphyrins screen the flux of photons reaching the underlying GaP (i.e., when the absorbed photon-to-current dye-contribution efficiency[65] is 0%) or where all excited-state cobalt porphyrins transfer carriers to the underlying GaP via a dye-sensitization mechanism (i.e., when the absorbed photon-to-current dye-contribution efficiency is 100%) (Figures 7, S7, and S8). These

https://dx.doi.org/10.1021/acsaem.0c00919
ACS Appl. Energy Mater. 2020, 3, 7512−7519

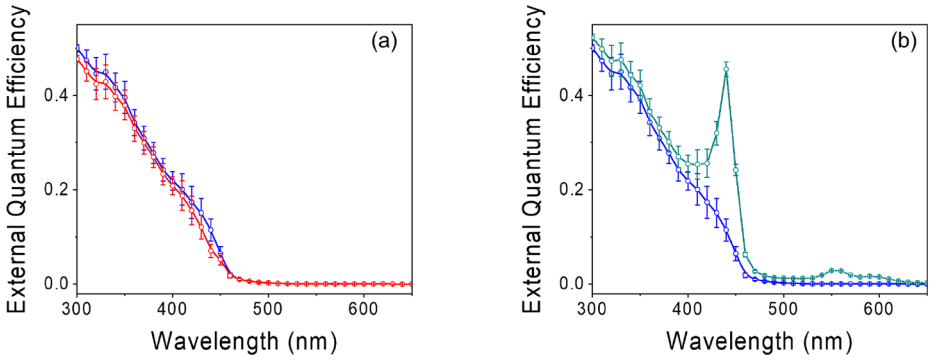

Figure 7. (a) Hypothetical external quantum efficiency action spectrum of a cobalt porphyrin−polypyridyl-modified GaP electrode constructed with the assumption that all immobilized porphyrins serve strictly as light-screening pigments (not catalysts) and all photons absorbed by the porphyrin layer are screened from the underlying GaP semiconductor (red). (b) Hypothetical external quantum efficiency action spectrum of a cobalt porphyrin−polypyridyl-modified GaP electrode constructed with the assumption that all immobilized porphyrins serve strictly as dye sensitizers (not catalysts) and all photons absorbed by the porphyrin layer contribute to production of photocurrent via a dye-sensitization mechanism (teal). For comparison, the external quantum efficiency action spectrum recorded using PPy|GaP electrodes polarized at 0 V vs RHE in 0.1 M phosphate buffer (blue) is included in both panels a and b.

hypothetical plots further demonstrate the measured enhancements in EQE following porphyrin modification cannot be accounted for by porphyrin dye sensitization. For example, the apparent absorbed photon-to-current dye-contribution efficiencies required to achieve the EQEs shown in Figure 4a exceed 250% (Figure S9; see the Supporting Information for further details). Although there is a clear increase in the ratio of electron flux (measured as current) to incident photon flux following porphyrin modification of the PPy|GaP electrodes that cannot be accounted for via mechanisms involving dye sensitization, the current data do not permit a further deconvolution of enhancements arising from chemical catalysis and/or changes in surface energetics.[66−70] In principle, the analysis described in this work can be applied to other molecular-modified semiconductor assemblies if information is available regarding their EQEs and LHEs as well as the surface loadings and extinction coefficients of the molecular components.

4. CONCLUSION

In conclusion, optical and photoelectrochemical measurements, including determination of light harvesting efficiencies and in operando quantum efficiencies associated with hydrogen production, were performed using chemically modified GaP working electrodes. Our results indicate the immobilized porphyrins contribute relatively little to extending the photoactivity of these assemblies to wavelengths outside the actinic range of GaP yet are essential to improving the overall photocurrent density. Although this report focuses on better understanding the HER activity of metalloporphyrin-modified GaP semiconductors, the analysis techniques (including quantification of catalyst loading coupled with determination of the LHEs, EQEs, and IQEs obtained from measurements performed prior to and following catalyst-modification chemistry) can likely be applied to other photoelectrosynthetic assemblies and chemical transformations. Thus, this approach highlights a general yet useful strategy for better understanding the activity of photoelectrosynthetic assemblies containing catalysts that absorb visible light.

■ ASSOCIATED CONTENT

Supporting Information

The Supporting Information is available free of charge at https://pubs.acs.org/doi/10.1021/acsaem.0c00919.

Synthesis, optical characterization, photoelectrochemical data, and calculations for the apparent absorbed photon-to-current dye-contribution efficiencies (PDF)

■ AUTHOR INFORMATION

Corresponding Author

Gary F. Moore − *School of Molecular Sciences and the Biodesign Institute Center for Applied Structural Discovery (CASD), Arizona State University, Tempe, Arizona 85287-1604, United States;* orcid.org/0000-0003-3369-9308; Email: gfmoore@asu.edu

Authors

Brian L. Wadsworth − *School of Molecular Sciences and the Biodesign Institute Center for Applied Structural Discovery (CASD), Arizona State University, Tempe, Arizona 85287-1604, United States;* orcid.org/0000-0002-0274-9993

Nghi P. Nguyen − *School of Molecular Sciences and the Biodesign Institute Center for Applied Structural Discovery (CASD), Arizona State University, Tempe, Arizona 85287-1604, United States*

Daiki Nishiori − *School of Molecular Sciences and the Biodesign Institute Center for Applied Structural Discovery (CASD), Arizona State University, Tempe, Arizona 85287-1604, United States*

Anna M. Beiler − *School of Molecular Sciences and the Biodesign Institute Center for Applied Structural Discovery (CASD), Arizona State University, Tempe, Arizona 85287-1604, United States*

Complete contact information is available at: https://pubs.acs.org/10.1021/acsaem.0c00919

Notes

The authors declare no competing financial interest.

■ ACKNOWLEDGMENTS

This research was supported by the National Science Foundation under an Early Career Award 1653982. G.F.M.

acknowledges support from the Camille Dreyfus Teacher-Scholar Awards Program. B.L.W. and A.M.B. were supported by an IGERT-SUN fellowship funded by the National Science Foundation (Grant 1144616) and the Phoenix Chapter of the ARCS Foundation. A.M.B received additional support from the P.E.O. Scholar Award.

■ ABBREVIATIONS

CoTTP, 5,10,15,20-tetra-*p*-tolylporphyrin cobalt(II)
EQE, external quantum efficiency
GaP, gallium phosphide
HER, hydrogen evolution reaction
IQE, internal quantum efficiency
LHE, light harvesting efficiency
PPy, polypyridyl
RHE, reversible hydrogen electrode
Φ_{abs}, probability of absorption
Φ_{inj}, probability of charge injection
Φ_{sep}, probability of charge separation

■ REFERENCES

(1) Ardo, S.; Fernandez Rivas, D.; Modestino, M. A.; Schulze Greiving, V.; Abdi, F. F.; Alarcon Llado, E.; Artero, V.; Ayers, K.; Battaglia, C.; Becker, J.-P.; Bederak, D.; Berger, A.; Buda, F.; Chinello, E.; Dam, B.; Di Palma, V.; Edvinsson, T.; Fujii, K.; Gardeniers, H.; Geerlings, H.; H. Hashemi, S. M.; Haussener, S.; Houle, F.; Huskens, J.; James, B. D.; Konrad, K.; Kudo, A.; Kunturu, P. P.; Lohse, D.; Mei, B.; Miller, E. L.; Moore, G. F.; Muller, J.; Orchard, K. L.; Rosser, T. E.; Saadi, F. H.; Schuttauf, J.-W.; Seger, B.; Sheehan, S. W.; Smith, W. A.; Spurgeon, J.; Tang, M. H.; van de Krol, R.; Vesborg, P. C. K.; Westerik, P. Pathways to Electrochemical Solar-Hydrogen Technologies. *Energy Environ. Sci.* **2018**, *11*, 2768−2783.
(2) Faunce, T. A.; Lubitz, W.; Rutherford, A. W.; MacFarlane, D.; Moore, G. F.; Yang, P.; Nocera, D. G.; Moore, T. A.; Gregory, D. H.; Fukuzumi, S.; Yoon, K. B.; Armstrong, F. A.; Wasielewski, M. R.; Styring, S. Energy and Environment Policy Case for a Global Project on Artificial Photosynthesis. *Energy Environ. Sci.* **2013**, *6*, 695−698.
(3) Hambourger, M.; Moore, G. F.; Kramer, D. M.; Gust, D.; Moore, A. L.; Moore, T. A. Biology and Technology for Photochemical Fuel Production. *Chem. Soc. Rev.* **2009**, *38*, 25−35.
(4) McKone, J. R.; Marinescu, S. C.; Brunschwig, B. S.; Winkler, J. R.; Gray, H. B. Earth-Abundant Hydrogen Evolution Electrocatalysts. *Chem. Sci.* **2014**, *5*, 865−878.
(5) Wadsworth, B. L.; Khusnutdinova, D.; Moore, G. F. Polymeric Coatings for Applications in Electrocatalytic and Photoelectrosynthetic Fuel Production. *J. Mater. Chem. A* **2018**, *6*, 21654−21665.
(6) Ye, R.; Zhao, J.; Wickemeyer, B. B.; Toste, F. D.; Somorjai, G. A. Foundations and Strategies of the Construction of Hybrid Catalysts for Optimized Performances. *Nat. Catal.* **2018**, *1*, 318−325.
(7) Queyriaux, N.; Kaeffer, N.; Morozan, A.; Chavarot-Kerlidou, M.; Artero, V. Molecular Cathode and Photocathode Materials for Hydrogen Evolution in Photoelectrochemical Devices. *J. Photochem. Photobiol., C* **2015**, *25*, 90−105.
(8) Bullock, R. M.; Das, A. K.; Appel, A. M. Surface Immobilization of Molecular Electrocatalysts for Energy Conversion. *Chem. - Eur. J.* **2017**, *23*, 7626−7641.
(9) Beiler, A. M.; Khusnutdinova, D.; Wadsworth, B. L.; Moore, G. F. Cobalt Porphyrin−Polypyridyl Surface Coatings for Photoelectrosynthetic Hydrogen Production. *Inorg. Chem.* **2017**, *56*, 12178−12185.
(10) Khusnutdinova, D.; Beiler, A. M.; Wadsworth, B. L.; Jacob, S. I.; Moore, G. F. Metalloporphyrin-Modified Semiconductors for Solar Fuel Production. *Chem. Sci.* **2017**, *8*, 253−259.
(11) Wadsworth, B. L.; Beiler, A. M.; Khusnutdinova, D.; Reyes Cruz, E. A.; Moore, G. F. Interplay between Light Flux, Quantum Efficiency, and Turnover Frequency in Molecular-Modified Photoelectrosynthetic Assemblies. *J. Am. Chem. Soc.* **2019**, *141*, 15932−15941.
(12) Wadsworth, B. L.; Khusnutdinova, D.; Urbine, J. M.; Reyes, A. S.; Moore, G. F. Expanding the Redox Range of Surface-Immobilized Metallocomplexes using Molecular Interfaces. *ACS Appl. Mater. Interfaces* **2020**, *12*, 3903−3911.
(13) Ladomenou, K.; Natali, M.; Iengo, E.; Charalampidis, G.; Scandola, F.; Coutsolelos, A. G. Photochemical Hydrogen Generation with Porphyrin-Based Systems. *Coord. Chem. Rev.* **2015**, *304*, 38−54.
(14) Costentin, C.; Robert, M.; Savéant, J. M. Current Issues in Molecular Catalysis Illustrated by Iron Porphyrins as Catalysts of the CO_2-to-CO Electrochemical Conversion. *Acc. Chem. Res.* **2015**, *48*, 2996−3006.
(15) Manbeck, G. F.; Fujita, E. A Review of Iron and Cobalt Porphyrins, Phthalocyanines and Related Complexes for Electrochemical and Photochemical Reduction of Carbon Dioxide. *J. Porphyrins Phthalocyanines* **2015**, *19*, 45−64.
(16) Morris, A. J.; Meyer, G. J.; Fujita, E. Molecular Approaches to the Photocatalytic Reduction of Carbon Dioxide for Solar Fuels. *Acc. Chem. Res.* **2009**, *42*, 1983−1994.
(17) Losse, S.; Vos, J. G.; Rau, S. Catalytic Hydrogen Production at Cobalt Centres. *Coord. Chem. Rev.* **2010**, *254*, 2492−2504.
(18) Collin, J. P.; Sauvage, J. P. Electrochemical Reduction of Carbon Dioxide Mediated by Molecular Catalysts. *Coord. Chem. Rev.* **1989**, *93*, 245−268.
(19) Dalle, K. E.; Warnan, J.; Leung, J. J.; Reuillard, B.; Karmel, I. S.; Reisner, E. Electro-and Solar-Driven Fuel Synthesis with First Row Transition Metal Complexes. *Chem. Rev.* **2019**, *119*, 2752−2875.
(20) Zhang, B.; Sun, L. Artificial Photosynthesis: Opportunities and Challenges of Molecular Catalysts. *Chem. Soc. Rev.* **2019**, *48*, 2216−2264.
(21) Morikawa, T.; Sato, S.; Sekizawa, K.; Arai, T.; Suzuki, T. M. Molecular Catalysts Immobilized on Semiconductor Photosensitizers for Proton Reduction toward Visible-Light-Driven Overall Water Splitting. *ChemSusChem* **2019**, *12*, 1807−1824.
(22) Auwärter, W.; Écija, D.; Klappenberger, F.; Barth, J. V. Porphyrins at Interfaces. *Nat. Chem.* **2015**, *7*, 105−120.
(23) Gust, D.; Moore, T. A.; Moore, A. L. Solar Fuels via Artificial Photosynthesis. *Acc. Chem. Res.* **2009**, *42*, 1890−1898.
(24) Lindsey, J. S.; Bocian, D. F. Molecules for Charge-Based Information Storage. *Acc. Chem. Res.* **2011**, *44*, 638−650.
(25) Swierk, J. R.; Mendez-Hernandez, D. D.; McCool, N. S.; Liddell, P.; Terazono, Y.; Pahk, I.; Tomlin, J. J.; Oster, N. V.; Moore, T. A.; Moore, A. L.; Gust, D.; Mallouk, T. E. Metal-Free Organic Sensitizers for Use in Water-Splitting Dye-Sensitized Photoelectrochemical Cells. *Proc. Natl. Acad. Sci. U. S. A.* **2015**, *112*, 1681−1686.
(26) Higashino, T.; Imahori, H. Porphyrins as Excellent Dyes for Dye-Sensitized Solar Cells: Recent Developments and Insights. *Dalton Trans.* **2015**, *44*, 448−463.
(27) Mathew, S.; Yella, A.; Gao, P.; Humphry-Baker, R.; Curchod, B. F.; Ashari-Astani, N.; Tavernelli, I.; Rothlisberger, U.; Nazeeruddin, M. K.; Grätzel, M. Dye-Sensitized Solar Cells with 13% Efficiency Achieved through the Molecular Engineering of Porphyrin Sensitizers. *Nat. Chem.* **2014**, *6*, 242−247.
(28) Walter, M. G.; Rudine, A. B.; Wamser, C. C. Porphyrins and Phthalocyanines in Solar Photovoltaic Cells. *J. Porphyrins Phthalocyanines* **2010**, *14*, 759−792.
(29) Li, L. L.; Diau, E. W. G. Porphyrin-Sensitized Solar Cells. *Chem. Soc. Rev.* **2013**, *42*, 291−304.
(30) Standing, A.; Assali, S.; Gao, L.; Verheijen, M. A.; Van Dam, D.; Cui, Y.; Notten, P. H.; Haverkort, J. E.; Bakkers, E. P. Efficient Water Reduction with Gallium Phosphide Nanowires. *Nat. Commun.* **2015**, *6*, 7824.
(31) Liu, C.; Sun, J.; Tang, J.; Yang, P. Zn-Doped p-Type Gallium Phosphide Nanowire Photocathodes from a Surfactant-Free Solution Synthesis. *Nano Lett.* **2012**, *12*, 5407−5411.
(32) Barton, E. E.; Rampulla, D. M.; Bocarsly, A. B. Selective Solar-Driven Reduction of CO_2 to Methanol Using a Catalyzed p-GaP

https://dx.doi.org/10.1021/acsaem.0c00919
ACS Appl. Energy Mater. 2020, 3, 7512−7519

Based Photoelectrochemical Cell. *J. Am. Chem. Soc.* **2008**, *130*, 6342−6344.
(33) Grätzel, M. Photoelectrochemical Cells. *Nature* **2001**, *414*, 338−344.
(34) Butler, M. A.; Ginley, D. S. P-Type GaP as a Semiconducting Photoelectrode. *J. Electrochem. Soc.* **1980**, *127*, 1273−1278.
(35) Halmann, M. Photoelectrochemical Reduction of Aqueous Carbon Dioxide on p-Type Gallium Phosphide in Liquid Junction Solar Cells. *Nature* **1978**, *275*, 115−116.
(36) Tomkiewicz, M.; Woodall, J. M. Photoassisted Electrolysis of Water by Visible Irradiation of a p-Type Gallium Phosphide Electrode. *Science* **1977**, *196*, 990−991.
(37) Bockris, J. M.; Uosaki, K. The Rate of the Photoelectrochemical Generation of Hydrogen at p-Type Semiconductors. *J. Electrochem. Soc.* **1977**, *124*, 1348−1355.
(38) Krawicz, A.; Yang, J.; Anzenberg, E.; Yano, J.; Sharp, I. D.; Moore, G. F. Photofunctional Construct that Interfaces Molecular Cobalt-Based Catalysts for H_2 Production to a Visible-Light-Absorbing Semiconductor. *J. Am. Chem. Soc.* **2013**, *135*, 11861−11868.
(39) Gleria, M.; Memming, R. Charge Transfer Processes at Large Band Gap Semiconductor Electrodes: Reactions at SiC-Electrodes. *J. Electroanal. Chem.* **1975**, *65*, 163−175.
(40) Memming, R.; Schwandt, G. Electrochemical Properties of Gallium Phosphide in Aqueous Solutions. *Electrochim. Acta* **1968**, *13*, 1299−1310.
(41) Liang, X.; Cao, X.; Sun, W.; Ding, Y. Recent Progress in Visible Light Driven Water Oxidation using Semiconductors Coupled with Molecular Catalysts. *ChemCatChem* **2019**, *11*, 6190−6202.
(42) Trotochaud, L.; Mills, T. J.; Boettcher, S. W. An Optocatalytic Model for Semiconductor−Catalyst Water-Splitting Photoelectrodes Based on in situ Optical Measurements on Operational Catalysts. *J. Phys. Chem. Lett.* **2013**, *4*, 931−935.
(43) Kempler, P. A.; Gonzalez, M. A.; Papadantonakis, K. M.; Lewis, N. S. Hydrogen Evolution with Minimal Parasitic Light Absorption by Dense Co−P Catalyst Films on Structured p-Si Photocathodes. *ACS Energy Lett.* **2018**, *3*, 612−617.
(44) Chen, H. Y.; Ardo, S. Direct Observation of Sequential Oxidations of a Titania-Bound Molecular Proxy Catalyst Generated Through Illumination of Molecular Sensitizers. *Nat. Chem.* **2018**, *10*, 17−23.
(45) Beiler, A. M.; Moore, G. F. Multi-Electron Transfer Photochemistry: Caught in the Act. *Nat. Chem.* **2018**, *10*, 3−4.
(46) Willkomm, J.; Orchard, K. L.; Reynal, A.; Pastor, E.; Durrant, J. R.; Reisner, E. Dye-Sensitised Semiconductors Modified with Molecular Catalysts for Light-Driven H_2 Production. *Chem. Soc. Rev.* **2016**, *45*, 9−23.
(47) Ashford, D. L.; Gish, M. K.; Vannucci, A. K.; Brennaman, M. K.; Templeton, J. L.; Papanikolas, J. M.; Meyer, T. J. Molecular Chromophore−Catalyst Assemblies for Solar Fuel Applications. *Chem. Rev.* **2015**, *115*, 13006−13049.
(48) Brennaman, M. K.; Dillon, R. J.; Alibabaei, L.; Gish, M. K.; Dares, C. J.; Ashford, D. L.; House, R. L.; Meyer, G. J.; Papanikolas, J. M.; Meyer, T. J. Finding the Way to Solar Fuels with Dye-Sensitized Photoelectrosynthesis Cells. *J. Am. Chem. Soc.* **2016**, *138*, 13085−13102.
(49) Ilic, S.; Brown, E. S.; Xie, Y.; Maldonado, S.; Glusac, K. D. Sensitization of p-GaP with Monocationic Dyes: The Effect of Dye Excited-State Lifetime on Hole Injection Efficiencies. *J. Phys. Chem. C* **2016**, *120*, 3145−3155.
(50) Memming, R.; Tributsch, H. Electrochemical Investigations on the Spectral Sensitization of Gallium Phosphide Electrodes. *J. Phys. Chem.* **1971**, *75*, 562−570.
(51) Hammarström, L. Accumulative Charge Separation for Solar Fuels Production: Coupling Light-Induced Single Electron Transfer to Multielectron Catalysis. *Acc. Chem. Res.* **2015**, *48*, 840−850.
(52) LHE defines the fraction of incident photons that are absorbed by a material and is synonymous with the terms absorptance and probability of absorption (Φ_{abs}).
(53) Chen, Z.; Jaramillo, T. F.; Deutsch, T. G.; Kleiman-Shwarsctein, A.; Forman, A. J.; Gaillard, N.; Garland, R.; Takanabe, K.; Heske, C.; Sunkara, M.; McFarland, E. W.; et al. Accelerating Materials Development for Photoelectrochemical Hydrogen Production: Standards for Methods, Definitions, and Reporting Protocols. *J. Mater. Res.* **2010**, *25*, 3−16.
(54) Döscher, H.; Young, J. L.; Geisz, J. F.; Turner, J. A.; Deutsch, T. G. Solar-to-Hydrogen Efficiency: Shining Light on Photoelectrochemical Device Performance. *Energy Environ. Sci.* **2016**, *9*, 74−80.
(55) EQE, also known as incident photon-to-current efficiency (IPCE), is the ratio of electron flux measured as current to incident photon flux.
(56) IQE, also known as absorbed photon-to-current efficiency (APCE), is the ratio of electron flux measured as current to absorbed photon flux.
(57) LHE is a component of EQE, where EQE is the product of LHE (which is the probability of absorption, Φ_{abs}), probability of charge separation (Φ_{sep}), and probability of charge injection (Φ_{inj}).
(58) Lacey, S. D. The Absorption Coefficient of Gallium Phosphide in the Wavelength Region 530 to 1100 nm. *Solid State Commun.* **1970**, *8*, 1115−1118.
(59) At the time of writing, the air mass 1.5 global tilt (AM 1.5 G) spectrum from the ASTM G-173-03 data set is available online at https://www.nrel.gov/grid/solar-resource/spectra.html (accessed November 12, 2019).
(60) Changes in the electronic spectra of cobalt porphyrins when in the presence of pyridine and oxygen have been previously reported and ascribed to axial coordination of a pyridine unit and a superoxide ion. See refs 62, 63, and 64.
(61) Given the $\Phi_{trans} \sim 0$ at 440 nm for all samples and LHE is not directly measured but is determined from reflectance and transmittance measurements, any differences in LHE at 440 nm correspond to changes in reflection properties following porphyrin modification. Nonetheless, the LHE data indicate any decrease in LHE at 440 nm following porphyrin modification is limited to <1%.
(62) Walker, F. A. Electron Spin Resonance Study of Coordination to the Fifth and Sixth Positions of $\alpha,\beta,\gamma,\delta$-Tetra(p-methoxyphenyl)-porphinatocobalt (II). *J. Am. Chem. Soc.* **1970**, *92*, 4235−4244.
(63) Walker, F. A. Steric and Electronic Effects in the Coordination of Amines to a Cobalt (II) Porphyrin. *J. Am. Chem. Soc.* **1973**, *95*, 1150−1153.
(64) Walker, F. A. Reactions of Monomeric Cobalt-Oxygen Complexes. I. Thermodynamics of Reaction of Molecular Oxygen with Five-and Six-Coordinate Amine Complexes of a Cobalt Porphyrin. *J. Am. Chem. Soc.* **1973**, *95*, 1154−1159.
(65) Honda, S.; Ohkita, H.; Benten, H.; Ito, S. Multi-Colored Dye Sensitization of Polymer/Fullerene Bulk Heterojunction Solar Cells. *Chem. Commun.* **2010**, *46*, 6596−6598.
(66) Barroso, M.; Cowan, A. J.; Pendlebury, S. R.; Grätzel, M.; Klug, D. R.; Durrant, J. R. The Role of Cobalt Phosphate in Enhancing the Photocatalytic Activity of α-Fe_2O_3 Toward Water Oxidation. *J. Am. Chem. Soc.* **2011**, *133*, 14868−14871.
(67) Barroso, M.; Mesa, C. A.; Pendlebury, S. R.; Cowan, A. J.; Hisatomi, T.; Sivula, K.; Grätzel, M.; Klug, D. R.; Durrant, J. R. Dynamics of Photogenerated Holes in Surface Modified α-Fe_2O_3 Photoanodes for Solar Water Splitting. *Proc. Natl. Acad. Sci. U. S. A.* **2012**, *109*, 15640−15645.
(68) Li, W.; He, D.; Sheehan, S. W.; He, Y.; Thorne, J. E.; Yao, X.; Brudvig, G. W.; Wang, D. Comparison of Heterogenized Molecular and Heterogeneous Oxide Catalysts for Photoelectrochemical Water Oxidation. *Energy Environ. Sci.* **2016**, *9*, 1794−1802.
(69) Thorne, J. E.; Jang, J. W.; Liu, E. Y.; Wang, D. Understanding the Origin of Photoelectrode Performance Enhancement by Probing Surface Kinetics. *Chem. Sci.* **2016**, *7*, 3347−3354.
(70) Klahr, B.; Gimenez, S.; Fabregat-Santiago, F.; Bisquert, J.; Hamann, T. W. Electrochemical and Photoelectrochemical Investigation of Water Oxidation with Hematite Electrodes. *Energy Environ. Sci.* **2012**, *5*, 7626−7636.

https://dx.doi.org/10.1021/acsaem.0c00919
ACS Appl. Energy Mater. 2020, 3, 7512−7519